Supporting Information:

Rising reductive Fe(II)/Co(II) sites on P-doped $FeCo_2O_{4-x}$ nanosheets to accelerate the valance cycle for the electroanalysis of As(III)

Yuan-Fan Yang,[a,b] Hong-Qi Huang,[a] Zong-Yin Song,[a,b] Hui-Quan Li,[c] Xin-Yu Yu,[d] Yu-Min Cui,[c,*] Meng Yang, [a,*] Shi-Hua Chen,[a,*] Xing-Jiu Huang,[a,b,*]

[a] Key Laboratory of Environmental Optics and Technology, And Environmental Materials and Pollution Control Laboratory, Institute of Solid State Physics, HFIPS, Chinese Academy of Sciences, Hefei 230031, China

[b] Department of Materials Science and Engineering, University of Science and Technology of China, Hefei 230026, China

[c] Anhui Provincial Key Laboratory for Degradation and Monitoring of Pollution of the Environment, School of Chemistry and Materials Engineering, Fuyang Normal University, Fuyang 236037, P.R. China

[d] Anhui Haoyuan Chemical Group Co., Ltd., Fuyang 236146, P.R. China

* Corresponding author

E-mail addresses: cymlh@126.com; myang@iim.ac.cn; chenshh@issp.ac.cn; xingjiuhuang@iim.ac.cn;

Tel.: +86 551 6559 1167; *Fax:*+86 551 6559 2420.

Contents

1. Experimental Section

1.1. Material Characterization.

1.2. Fabrication of Modified Electrodes.

2. Figures

Fig. S1. $FeCo_2O_{4-x}$: (a) SEM image, (b) element mapping images.

Fig. S2. N_2 adsorption-desorption isotherms of (a) $FeCo_2O_{4-x}$; (b) P- $FeCo_2O_{4-x}$; Pore size distributions of (c) $FeCo_2O_{4-x}$; (d) P- $FeCo_2O_{4-x}$.

Fig. S3. EDS pattern and elegmental content of P- $FeCo_2O_{4-x}$.

Fig. S4. Thermogravimetric analysis in air atmophere of P-$FeCo_2O_{4-x}$ and $FeCo_2O_{4-x}$.

Fig. S5. Full XPS spectrum of P-$FeCo_2O_{4-x}$ and $FeCo_2O_{4-x.}$

Fig. S6. (a) CV and (b) EIS of $FeCo_2O_{4-x}$ and P-$FeCo_2O_{4-x.}$

Fig. S7. SWASV conditions optimization with 5 ppb As(III) on P-$FeCo_2O_{4-x}$/GCE. Individually change: (a) buffer solution, (b) pH value, (c) deposition potential, and (d) deposition time.

Fig. S8. XRD patterns and SEM (inset) of (a) P-Co_3O_4, (b) P-Fe_2O_3; EDS pattern of (c) P-Co_3O_4, (d) P-Fe_2O_3; SWASV responses for detecting As(III) of (c) P-Co_3O_4, (d) P-Fe_2O_3.

Fig. S9. SWASV responses of P-$FeCo_2O_{4-x}$ and corrsponding linear equations toward different HMIs. (a-b) Cu(II), (c-d) Hg (II), (e-f) Cd(II), and (g-h) Pb (II).

Fig. S10. XPS spectra of (a) As 3d after deposition; (b) As 3d after SWASV; (c) Fe 2p after deposition; (d) Fe 2p after SWASV; (e) Co 2p after deposition; (f) Co 2p after SWASV.

3. Table

Table. S1. The proportion of Co(II), Co(III), Fe(II), and Fe(III) in the XPS spectra.

1. Experimental Section

1.1. Material Characterization.

Field-emission scanning electron microscopy (FESEM, Quanta 200 FEG, FEI Company, USA), was utilized for the morphology characterization of the prepared nanomaterials. Transmission electron microscopy (TEM), high-resolution TEM(HR-TEM) and energy-dispersive spectrometer (EDS) were carried out with a JEM-2010 transmission electron microscope operating at 200 kV (quantitative method, Cliff Lorimer thin ratio section). X-ray diffraction patterns (XRD) of the nanomaterials were performed with a Philips X'PertPro X-ray diffractometer (Cu Kα radiation λ=1.5418 Å). X-ray photoelectron spectroscopy (XPS) measurements were achieved using a VGESCALAB MKII spectrometer with an Mg Kα X-ray source (1253.6 eV, 120 W). Raman spectra were obtained by a Lab RAM HR800 confocal microscope Raman system (Horiba Jobin Yvon, Inc., USA). Fourier transform infrared spectrometer (FTIR) were recorded the infrared spectra between 0 and 4500 cm^{-1} (Magna-IR 750, Nicolet Instrument Co.). Thermal gravimetric analyzer monitors the mass change trend of the sample in the temperature range of 20-800 ^{o}C under the condition of nitrogen (Pyris 1, Perkin-Elmer Co). Brunauer-Emmett-Teller (BET) measurements were recorded with a specific surface area and porosity analyzer (ASAP2460).

All electrochemical measurements were performed with a CHI 760E computer-controlled potentiostat (ChenHua Instruments Co., Shanghai, China), including a standard three-electrode system, with a platinum wire, Ag/AgCl (3 mol L^{-1} KCl) electrode and a bare or modified glassy carbon electrode (GCE) as the counter electrode, reference electrode and the working electrode, respectively.

1.2. Fabrication of Modified Electrodes

Firstly, it was necessary to polish the GCE with talcum powder. The treated electrode surface was rinsed using deionized water and then immersed into diluted HNO_3, ethanol, and deionized with sonication for 15 s. The diameter of GCE is 3 mm, so that the geometrical area of the GCE is about 0.0707 cm^2. In addition, to obtain a homogeneous suspension, ultrasonic agitation was implemented to absolutely disperse 5 mg of the prepared sample into 5 ml of ultrapure water. Then 6.0 μL of the 1 mg ml^{-1} suspension above was pipetted onto the surface of GCE. Finally, the modified electrodes were placed for 12 h to dry.

2. Figures

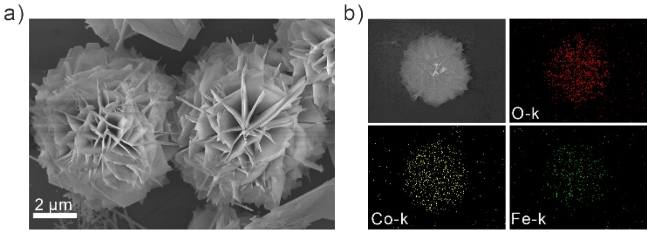

Fig. S1. $FeCo_2O_{4-x}$: (a) SEM image, (b) element mapping images.

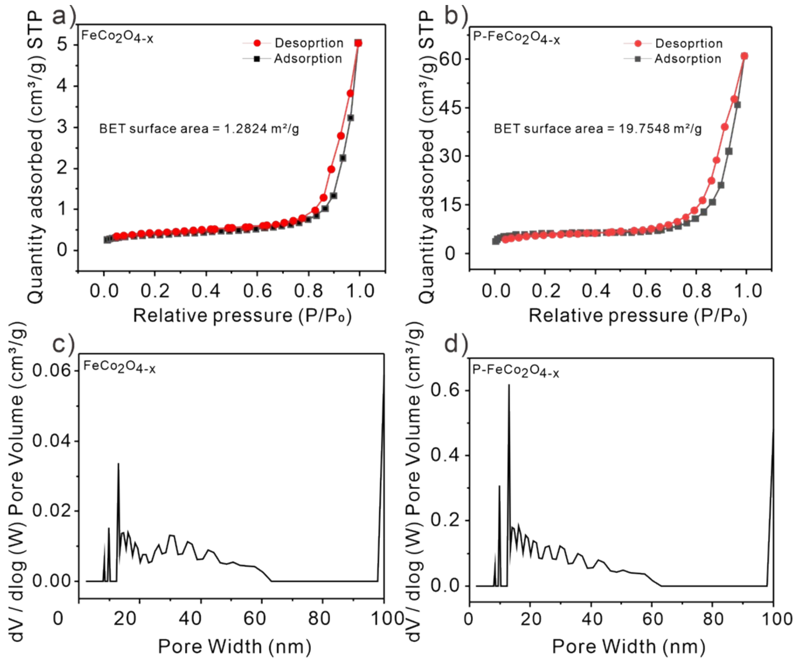

Fig. S2. N_2 adsorption-desorption isotherms of (a) $FeCo_2O_{4-x}$; (b) P-$FeCo_2O_{4-x}$; Pore size distributions of (c) $FeCo_2O_{4-x}$; (d) P-$FeCo_2O_{4-x}$.

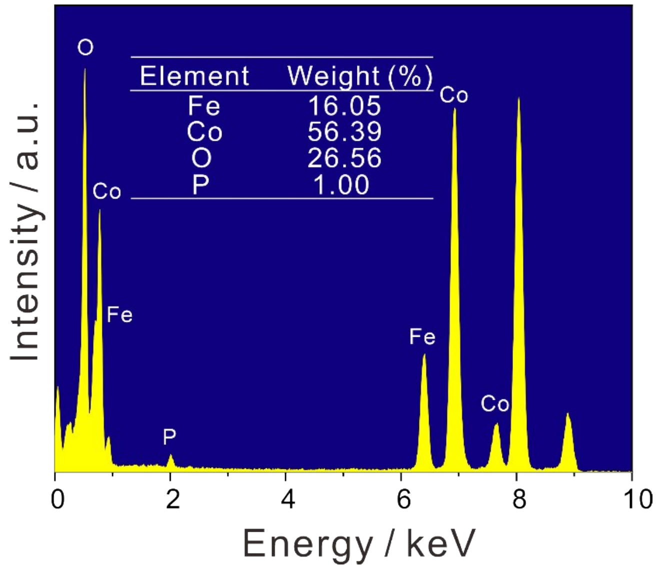

Element	Weight (%)
Fe	16.05
Co	56.39
O	26.56
P	1.00

Fig. S3. EDS pattern and elemental content of P-$FeCo_2O_{4-x}$.

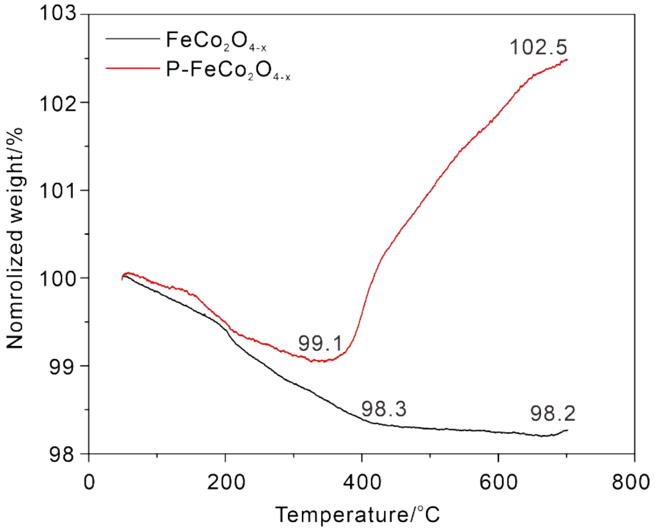

Fig. S4. Thermogravimetric analysis in air atmophere of P-$FeCo_2O_{4-x}$ and $FeCo_2O_{4-x}$.

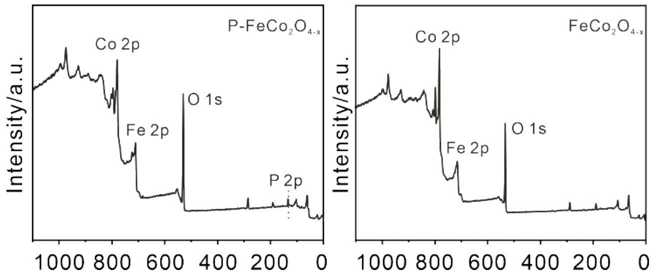

Fig. S5. Full XPS spectrum of P-$FeCo_2O_{4-x}$ and $FeCo_2O_{4-x}$.

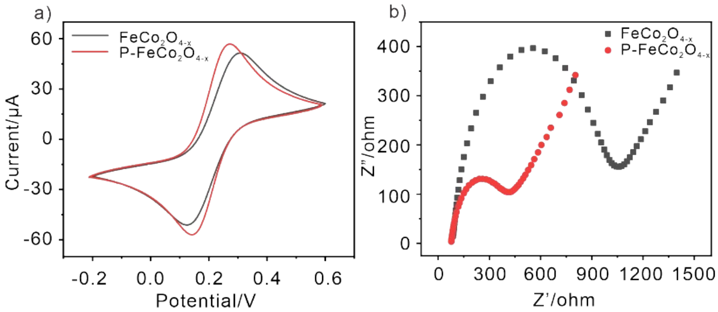

Fig. S6. (a) CV and (b) EIS of $FeCo_2O_{4-x}$ and P-$FeCo_2O_{4-x}$.

Electrochemical behaviors of $FeCo_2O_{4-x}$ nanomaterials before and after P-doping were recorded using cyclic voltammetry (CV) and electrical impedance spectroscopy (EIS). Cyclic voltammetry (CV) and Electrochemical impedance spectroscopy (EIS) were tested in 0.1 M KCl including 5 mM $K_3Fe(CN)_6$. Besides, for EIS, the applied potential was set as the average value of the peak potential obtained by the CV test, with a scan rate of 0.1 V/s, frequency range from 1 to 100000 Hz, and amplitude of 0.005 V. The higher peak current and lower ΔE of the P-$FeCo_2O_{4-x}$ nanosheets indicate a faster electron transfer rate. The charge transport process of $FeCo_2O_{4-x}$/GCE and P-$FeCo_2O_{4-x}$/GCE were investigated using EIS. The charge transfer resistance of P-$FeCo_2O_{4-x}$/GCE is almost 2 times lower than $FeCo_2O_{4-x}$/GCE, indicating a better electron transfer process between the electrolyte and the P-$FeCo_2O_{4-x}$/GCE. From the CV and EIS studies, it can be seen that the conductivity of P-$FeCo_2O_{4-x}$/GCE is enhanced.

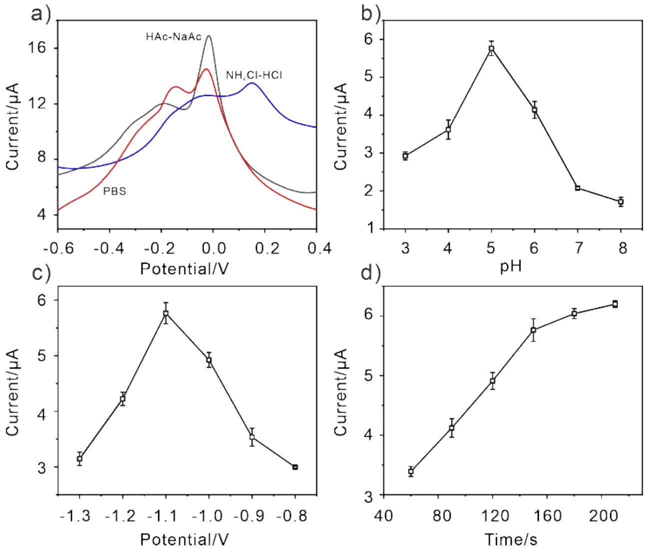

Fig. S7. SWASV conditions optimization with 5 ppb As(III) on P-$FeCo_2O_{4-x}$/GCE . Individually change: (a) buffer solution, (b) pH value, (c) deposition potential, and (d) deposition time.

To obtain the best sensitivity of P-$FeCo_2O_{4-x}$/GCE for the electrochemical detection of As(III), some key parameters (such as supporting electrolyte, pH, deposition potential, and enrichment time) are evaluated. The optimized design of the electrochemical variables is as Fig. S7. Screening from three common supporting electrolytes (HAc-NaAc, $NH_3 \cdot H_2O$, and PBS). When the supportive electrolyte solution is HAc-NaAc, the highest peak current is significantly better than the other two supporting electrolyte solutions, so HAc-NaAc was chosen as the supporting electrolyte for subsequent experiments. To examine the effect of the pH of the solution on peak current, pH 3.0 to pH 8.0 were investigated. At low pH, the peak current increases rapidly, and the peak reaches a maximum at pH 5; at high pH, the peak current decreases, which can be explained by the morphological changes in the presence of As(III). The modified electrode detects As(III) in 0.1 M HAc-NaAc (pH 5), with deposition potential varying from -0.8 V to -1.3 V. From -0.8 V to -1.1 V, the more negative the deposition potential, the more As(III) was reduced to As(0), and the electrochemical signal was enhanced. However, when the deposition potential exceeds -1.1 V, H_2 bubbles are generated on the surface of the modified electrode material, which hinders the contact between As(0) and the modified electrode, decreasing the electrochemical signal. The effect of preconcentration time (60 to 210 s) on peak voltammetric currents analyzed in 0.1 M HAc-NaAc (pH 5) solutions. The increase of the preconcentration time from 40 s to 150 s is proportional to the rise in the As(III) square wave peak response due to many free sites on the electrochemical surface. Beyond 150 s, the peak current response decreases due to the saturated deposition of As(III) on the electrochemical surface, which reduces the electron transport rate at the solution/electrode interface.

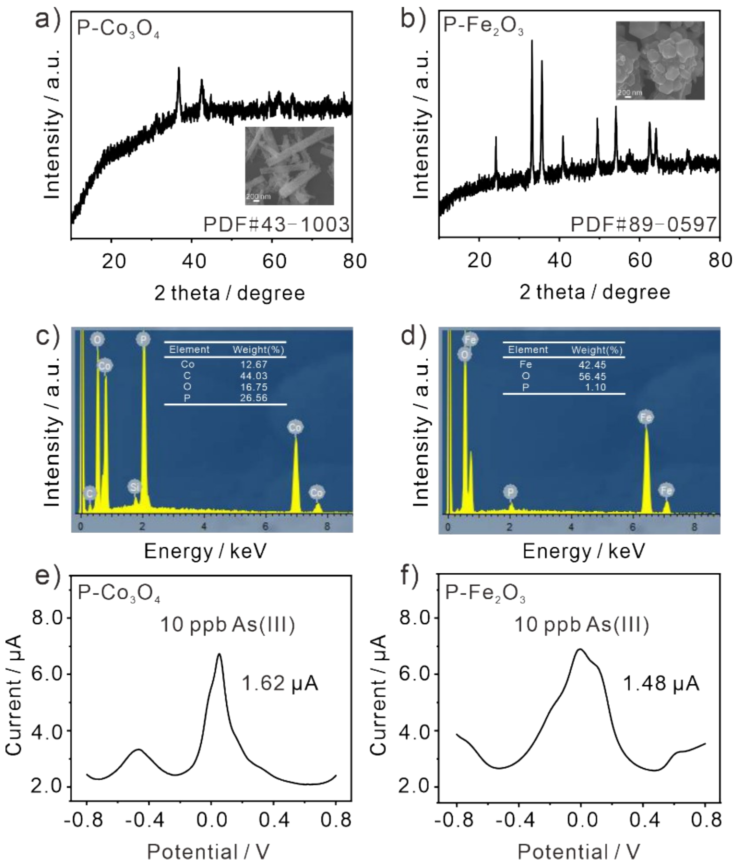

Fig. S8. XRD patterns and SEM (inset) of (a) P-Co_3O_4, (b) P-Fe_2O_3; EDS pattern of (c) P-Co_3O_4, (d) P-Fe_2O_3; SWASV responses for detecting As(III) of (c) P-Co_3O_4, (d) P-Fe_2O_3.

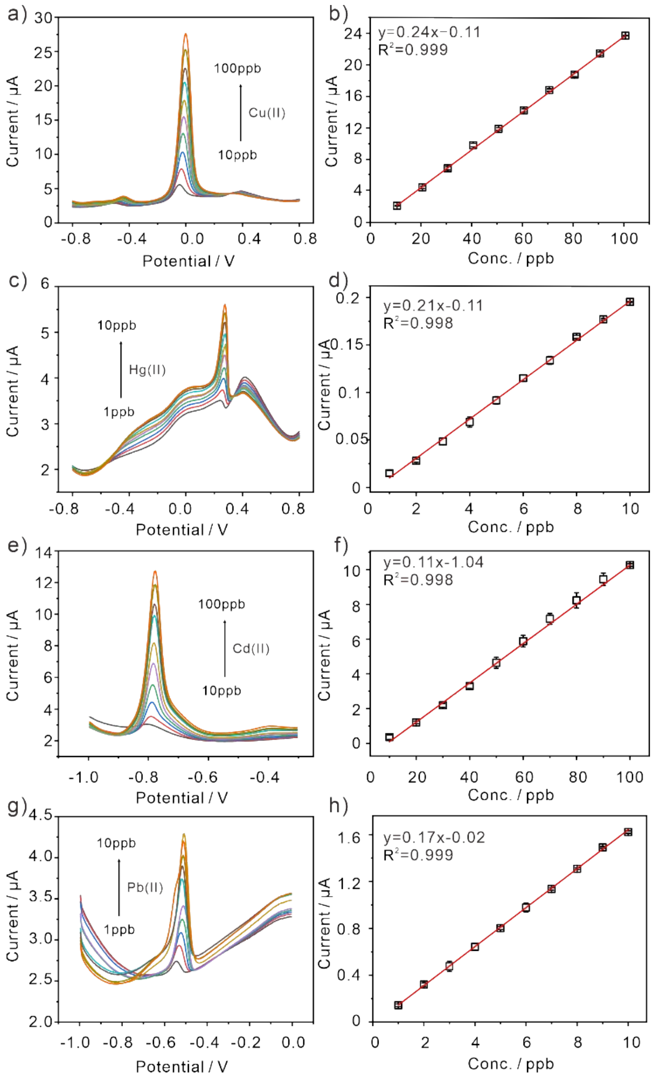

Fig. S9. SWASV responses of P-$FeCo_2O_{4-x}$ and corrsponding linear equations toward different HMIs. (a-b) Cu(II), (c-d) Hg (II), (e-f) Cd(II), and (g-h) Pb (II).

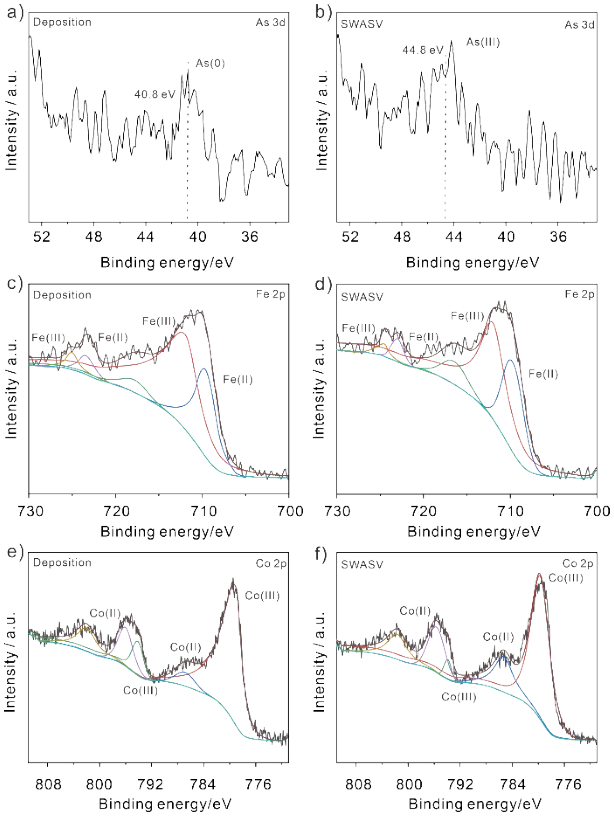

Fig. S10. XPS spectra of (a) As 3d after deposition; (b) As 3d after SWASV; (c) Fe 2p after deposition; (d) Fe 2p after SWASV; (e) Co 2p after deposition; (f) Co 2p after SWASV.

3. Table

Table S1. The proportion of Co(II), Co(III), Fe(II), and Fe(III) in the XPS spectra.

Sample	**Co(II)/Co$_{total}$**	**Co(III)/Co$_{total}$**	**Fe(II)/Fe$_{total}$**	**Fe(III)/Fe$_{total}$**
$FeCo_2O_{4-x}$	23.56%	76.44%	50.79%	49.21%
P-$FeCo_2O_{4-x}$	38.35%	61.65%	62.70%	37.30%
P-$FeCo_2O_{4-x}$-As(III)	29.21%	70.79%	58.25%	41.75%